MOCVD AlYN/GaN HEMTs with 66.5 mV/decade sub-threshold swing and 10^9 on/off ratio

Cite as: Appl. Phys. Lett. **126**, 223509 (2025); doi: 10.1063/5.0257333
Submitted: 9 January 2025 · Accepted: 16 May 2025 ·
Published Online: 6 June 2025

Kazuki Nomoto,[1] Isabel Streicher,[2,a)] Thai-Son Nguyen,[3] Chandrashekhar Savant,[3] Madhav Ramesh,[1] Siyuan Ma,[3] Jimy Encomendero,[1] Lutz Kirste,[2] Patrik Straňák,[2] Ruediger Quay,[2] Stefano Leone,[2] Huili Grace Xing,[1,3,4] and Debdeep Jena[1,3,4]

AFFILIATIONS

[1]School of Electrical and Computer Engineering, Cornell University, Ithaca, New York 14853, USA
[2]Fraunhofer Institute for Applied Solid State Physics IAF, Tullastrasse 72, 79108 Freiburg, Germany
[3]Department of Materials Science and Engineering, Cornell University, Ithaca, New York 14853, USA
[4]Kavli Institute at Cornell for Nanoscale Science, Cornell University, Ithaca, New York 14853, USA

[a)]**Present address:** Consiglio Nazionale delle Ricerche—Istituto per la Microelettronica e Microsistemi (CNR-IMM), Strada VIII, n. 5–Zona Industriale, 95121 Catania, Italy. **Author to whom correspondence should be addressed:** kn383@cornell.edu

ABSTRACT

We report the realization and operation of AlYN/GaN high-electron-mobility transistors (HEMTs). Metal-organic chemical vapor deposition is used to deposit AlYN/GaN semiconductor heterostructures on 100 mm SiC substrates. Polarization-induced 2D electron gas channels formed in the heterostructure exhibit room-temperature mobility $>1300\,\mathrm{cm^2/V\,s}$, sheet density $>1.4\times10^{13}/\mathrm{cm}^2$, and sheet resistance $<350\,\Omega/\square$ with good uniformity. Micron-long gate length HEMTs fabricated using regrown n^+ GaN contacts demonstrate good DC performance with saturation drain current >0.4 A/mm, transconductance >0.3 S/mm, low threshold voltage $V_T=-2.0$ V, and a high on/off ratio surpassing 10^9. The drain current shows a nearly negligible hysteresis with the sweep of the gate voltage. Notably, the devices exhibit a near-Boltzmann limit sub-threshold swing of 66.5 mV/dec. These observations highlight the promise of AlYN/GaN HEMTs for high-performance electronic applications.

Published under an exclusive license by AIP Publishing. https://doi.org/10.1063/5.0257333

06 June 2025 13:06:53

The observation of 2D electron gases (2DEGs) at undoped AlGaN/GaN heterojunctions[1] enabled the RF amplifiers based on nitride semiconductors.[2] Understanding the origin of these 2DEGs in both metal-polar and N-polar AlGaN/GaN heterostructures due to polarization effects[3] laid the foundation for AlGaN/GaN high-electron mobility transistors (HEMTs) on both polarities. In the past two decades, AlGaN/GaN HEMTs have made a significant impact on high power RF amplifiers owing to their excellent speed due to the high-electron mobility and high-breakdown voltages arising from the large energy bandgap.[4] The high breakdown voltage and low on-resistance due to the high 2DEG mobility in the same heterostructures enable fast switching of high voltages, making AlGaN/GaN HEMTs quite revolutionary for power electronics.[5]

Today, there is a need for more robust epitaxial barrier materials because AlGaN/GaN HEMTs are approaching their performance limits in RF and power electronics. Next-generation epitaxial barriers must preserve the high 2DEG mobility and provide better scaling and breakdown than AlGaN to make an impact. The barrier must be a wider bandgap nitride semiconductor, which is either binary AlN or an alloy in which some of the Al atoms are replaced by isovalent atoms that have three electrons in the outermost shell. These elements are in groups 13 (B, In) and 3 (Sc, Y, La) of the periodic table. Pure AlN barrier HEMTs have been implemented, provided the AlN barrier thickness is kept below the strain-limited thickness.[6–8] For alloy barriers, in addition to the early demonstrated case of AlInN,[9] the practicality and novel features of the unconventional choices have been recently discussed.[10,11] Recently, the following epitaxial barrier/GaN combinations have been realized to produce 2DEGs such as AlBN,[12] AlScN,[13–19] and AlYN.[20,21] The ternary nitride barriers at typically reported compositions of lower than 18% Sc, 17% In, and 6.9% Y reported in this work offer a bandgap larger than the bandgap of AlGaN barrier with more than 70% Ga. Compared to AlGaN, these novel barrier materials also offer larger polarization discontinuity on GaN, large conduction band offset, and higher dielectric constant, making them a promising approach for enhancing device scaling and performance of next-generation high-performance GaN HEMTs. Among these,

Published under an exclusive license by AIP Publishing

AlScN/GaN HEMTs[14,18] and AlBN/GaN HEMTs[12] have been realized. In this work, we report the realization of AlYN/GaN HEMTs.

Figure 1(a) shows the layer structure of the AlYN barrier GaN HEMT that we have grown by metal-organic chemical vapor deposition (MOCVD) on semi-insulating (S.I.) 4H SiC substrates using a solid $(MCp)_3Y$ precursor for yttrium supplied by Dockweiler Chemicals.[22] We presented the details of the growth process in our recent reports[21,23] and compared the MOCVD growth of AlYN with that of AlScN.[24,25] For this work, we grew the $Al_{1-x}Y_xN$/GaN heterostructures on 100 mm semi-insulating 4H-SiC (0001) substrates with a nucleation layer consisting of a high-temperature AlN. As indicated in Fig. 1(a), we used an iron-doped GaN lower buffer layer to compensate for residual donor impurities,[26] followed by a non-intentionally doped GaN buffer layer. We then grew a 9.7 nm thick AlYN barrier with 6.9% Y on the GaN layer with a nominal AlN interlayer to improve barrier homogeneity.[27] We passivated the AlYN surface with *in situ* SiNx to avoid surface oxidation. The layer thicknesses and Y composition were verified using high-resolution x-ray diffraction (HRXRD), x-ray reflectivity (XRR), and time-of-flight secondary ion mass spectrometry (ToF-SIMS).

Figure 1(b) shows the surface morphology measured by atomic force microscope (AFM) in the tapping mode. We measured a root mean square (rms) average roughness of 0.67 nm over a $10 \times 10\,\mu m^2$ scan area on the AlYN surface after removal of the *in situ* SiNx cap by wet-etching. We determined the layer thicknesses and Y composition of the AlYN layer in the same manner as described in our prior reports. Thickness and *ex situ* wafer bow measurements pinpointed excellent thickness uniformities with a standard deviation below 4% and wafer bow below 15 μm on the whole 4-in. wafer. The sheet resistance map of a $Al_{1-x}Y_xN$/GaN heterostructure with a Y concentration of $y = 6.9\%$ having $R_s = 335\Omega/\square$ is shown in Fig. 1(c). R_s is homogeneous across the wafer with a standard deviation of 0.7% and an electron mobility of $\mu = 1358\,cm^2/V{\cdot}s$ with a standard deviation of 3%, corresponding to a 2DEG sheet density of $n_s = 1.37 \times 10^{13}/cm^2$. These values are at room temperature, indicating a high quality polarization-induced 2DEG channel is formed.

In Fig. 2(a), we have shown a schematic cross section of the fabricated AlYN/GaN HEMTs with regrown Ohmic n^+GaN Ohmic contacts, along with a top-view scanning electron microscope (SEM) image of a DC AlYN/GaN HEMT in Fig. 2(b). The device dimensions labeled in Fig. 2(a) were measured by SEM. Device fabrication started with recess etching in the lithographically defined source-drain regions with a regrowth mask, followed by a molecular beam epitaxy (MBE) regrowth of a ∼50 nm thick heavily Si-doped ($\sim 10^{20}/cm^3$) n^+GaN in the Ohmic contact region. The round surface marks are remnants of Ga droplets formed during the MBE regrowth of highly Si-doped n^+GaN under Ga-rich conditions. While the droplets were removed by HCl cleaning, the underlying marks remain visible on the surface. The polycrystalline GaN on the regrowth mask was lifted off with the mask. This was followed by device isolation with BCl_3 inductively coupled plasma (ICP) etching and source/drain Ohmic metallization with 20/150 nm of Ti/Au metal without annealing. Figure 2(c) shows the results of a transmission-line method (TLM) measurement of the contact resistance. The metal to regrown n^+GaN contact resistance is 0.05 Ω mm, whereas the n^+GaN to 2DEG contact resistance is $R_c = 0.22\,\Omega$ mm for the non-alloyed Ohmic contacts. We consider this to be on the high side for regrown contacts and should be significantly reduced in the future.

We performed room-temperature Hall effect measurements on processed van der Pauw patterns with regrown Ohmic contacts after the device fabrication and obtained 2DEG sheet density $n_s = 0.95 \times 10^{13}/cm^2$, mobility $\mu = 1360\,cm^2/V\,s$, and sheet resistance $R_s = 481\,\Omega/\square$ across different device dies of the wafer. This indicates a significant reduction in the 2DEG sheet charge density from $1.37 \times 10^{13}/cm^2 \rightarrow 0.95 \times 10^{13}/cm^2$ after the device fabrication process with regrown contacts. A control AlYN/GaN HEMT sample processed *without* the regrown contact process showed no significant change in the sheet charge, mobility, or sheet resistance.

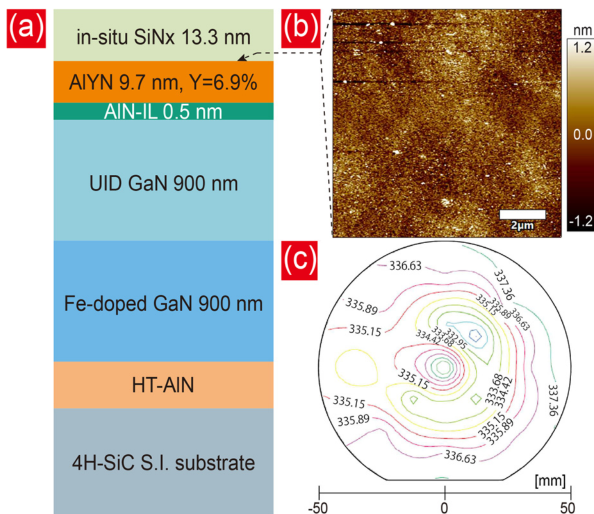

FIG. 1. (a) Epitaxial AlYN/GaN heterostructure realized by MOCVD and studied in this work. (b) AFM image of AlYN surface taken after removal of the *in situ* SiNx by wet-etching. (c) A sheet resistance map reveals a uniform sheet resistance of the 2D electron gas channel across the 100 mm wafer.

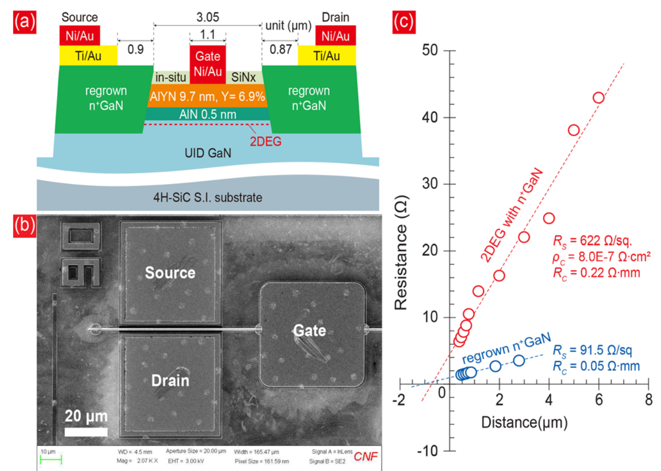

FIG. 2. (a) Schematic cross section of the fully processed AlYN/GaN HEMT on SiC substrate. (b) Post-fabrication top-view SEM of a DC HEMT. (c) Total resistance vs TLM spacing extracted at high current levels showing the contact and sheet resistances of the regrown region and the 2DEG channel.

06 June 2025 13:06:53

Published under an exclusive license by AIP Publishing

This suggests that the changes in sheet charge density are associated with specific steps involved in the regrowth process and post-regrowth treatments. The potential reasons could be due to the high temperature needed for regrowth[28] and associated changes in strain in the barrier. Though the exact mechanism for the decrease in the 2DEG density in the Ohmic regrowth process is not clear at this time and will be investigated and solved in the future, it is encouraging that the 2DEG *mobility* remains unchanged after the regrowth process.

We defined the gate electrodes by optical lithography, metal deposition of 30/250 nm Ni/Au metal stack, followed by a liftoff process. The AlYN/GaN HEMTs reported in this study have a source-to-drain spacing $L_{sd} = 3.0\,\mu$m, device-width $W_g = 50\,\mu$m, and a rectangular gate placed in the middle of the source-to-drain spacing with a gate length $L_g = 1.1\,\mu$m. Figure 3(a) shows the electrical output characteristics of the processed AlYN/GaN HEMT of Fig. 2, with a clean saturation of the drain current I_d, for gate bias V_{gs} stepped from +0.5 to −3.0 V, and drain bias V_{ds} sweep from 0 to 8 V. The saturation drain current density is 0.42 A/mm at $V_{gs} = 0.5$ V. We extracted the on-resistance of the AlYN/GaN HEMT from the linear region of the $I_d - V_{ds}$ curve at $V_{gs} = 0$ V to be $R_{on} = 3.77\,\Omega$ mm. The components of this on-resistance are[8,29] $R_{on} = 2R_c + 2R_{n^+GaN} + 2R_{int} + 2R_{ch,ac} + R_{ch,g}$, where R_c is the metal-n^+GaN contact resistance, R_{n^+GaN} is the resistance of the regrown n^+GaN from the edge of the Ohmic metal to the 2DEG interface, R_{int} is the interface resistance between the regrown GaN and the 2DEG, $R_{ch,ac}$ is the access region channel resistance from the source/drain to the gate edges, and $R_{ch,g}$ is the channel resistance under the gate.

From TLM measurements, we find the following contributions to R_{on}: $2R_c = 0.44\,\Omega$ mm, $2R_{n+GaN} = 0.32\,\Omega$ mm from the sheet resistance extracted from TLM measurements, and a total channel resistance $2R_{ch,ac} + R_{ch,g} = 1.90\,\Omega$ mm extracted using the measured TLM sheet resistance. The remaining portion $2R_{int} = 1.11\,\Omega$ mm of the total R_{on} is attributed to the interface resistance between the regrown GaN and the 2DEG. The dominant components of R_{on}, the channel resistance and the regrown interface resistance, suggests that the device output current can be improved significantly with a modified regrowth process and device scaling in the future.

Figure 3(b) shows the logscale transfer characteristics of the AlYN/GaN HEMTs with forward and reverse gate voltage sweeps at three drain voltages $V_{ds} = 1, 5,$ and 9 V. An $I_{on}/I_{off} > 10^9$ limited by gate leakage is measured, with negligible hysteresis. The drain-induced barrier lowering (DIBL) was measured over a wide drain bias range of 1–9 V. The value of the measured DIBL was ∼9 mV/V. The gate leakage current remained below $I_g = 10^{-9}$ A/mm for $V_{gs} < 0$, indicating that the AlYN barrier layer is highly effective in restricting gate leakage current to allow effective gate modulation of the AlYN/GaN HEMT.

Figure 3(c) shows the measured $I_d - V_{gs}$ transfer characteristics in the linear scale and the HEMT transconductance $g_m = \partial I_{\partial d}/\partial V_{gs}$. We observe sharp pinch-off characteristics with a low threshold voltage of $V_T = -1.12$, -1.03, and -1.05 V at the drain biases $V_{ds} = 1, 5,$ and 9 V obtained by linear extrapolation from the gate voltage at which the transconductance peaks. At a drain bias of $V_{ds} = 9$ V, a peak extrinsic transconductance of $g_m = 0.31$ S/mm is obtained.

We measured the capacitance–voltage ($C - V$) characteristics of the metal–insulator–semiconductor (MIS) capacitors of AlYN/AlN/GaN structure using circular Ni/Au pads with a 20 μm diameter as the anode and the 2DEG connected to the regrown contact as the cathode. Figure 3(d) shows the measured $C - V$ characteristic at 500 kHz at room temperature. The forward and reverse sweeps show a small hysteresis of 67 mV. Using the barrier thickness obtained from structural characterization, the relative dielectric constant of AlYN is extracted to be exceeding $\varepsilon_r = 10$ at 0 V across the frequency range of 10 kHz to 2 MHz. The sharp decrease in capacitance at negative voltage when the 2DEG depletes is consistent with the HEMT transfer characteristics seen in Fig. 3(c). The aforementioned results provide strong evidence that AlYN/AlN on GaN is an effective epitaxial gate dielectric with a decent relative dielectric constant that can simultaneously provide polarization-induced 2DEGs and appropriate insulating properties to serve as the gate barrier of AlYN/AlN/GaN HEMTs.

Figures 4(a) and 4(b) show the sub-threshold slopes (SSs) of the AlYN/GaN HEMTs for several V_{ds} bias voltages for upward and

06 June 2025 13:06:53

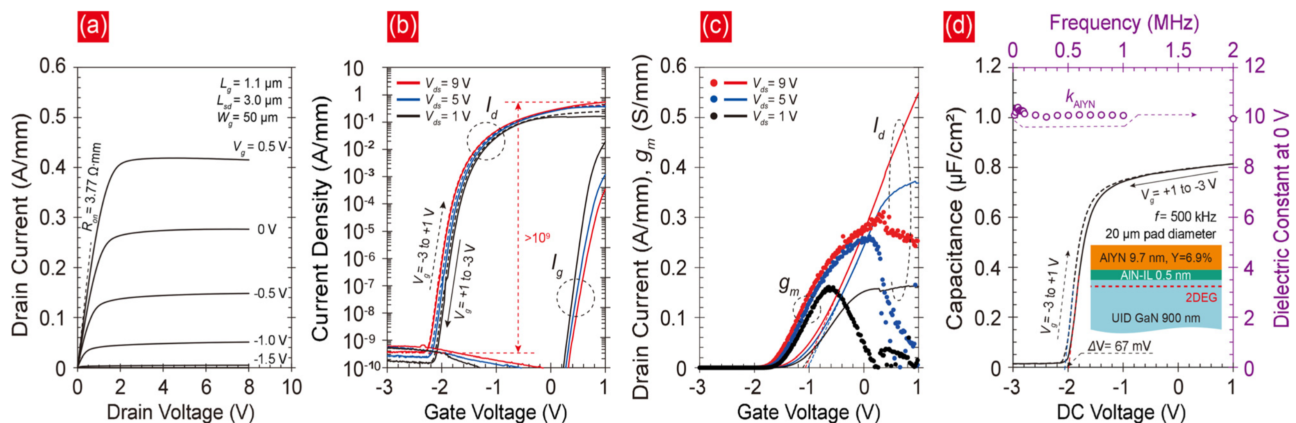

FIG. 3. (a) Measured DC output characteristics of the AlYN/GaN HEMT with regrown contacts showing an on resistance, $R_{on} = 3.77\Omega\cdot$mm with repeatable current saturation and a maximum $I_d = 0.42$ A/mm. (b) Log scale and (c) linear scale transfer characteristics showing an on/off drain current ratio exceeding nine orders of magnitude, and transconductance vs V_{gs} showing a peak transconductance of 0.31 S/mm at $V_{rmds} = 9$ V. (d) Measured $C - V$ characteristics of AlYN/AlN/GaN-based metal–insulator–semiconductor (MIS) capacitor at 500 kHz. Extracted dielectric constant across a frequency range of 10 kHz to 2 MHz of $\varepsilon_r > 10$ for AlYN (Y = 6.9%) with a 0.5 nm AlN inter layer extracted at 0 V.

Published under an exclusive license by AIP Publishing

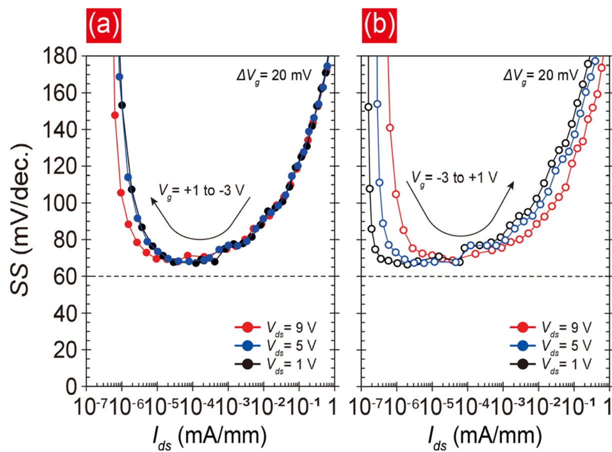

FIG. 4. The measured sub-threshold swing (SS) with multiple source-drain bias conditions: (a) SS for downward gate sweep, with a minimum value SS $\sim$67.2 mV/decade and (b) SS in the upward gate sweep with a minimum SS $\sim$66.5 mV at the drain bias of 1 V.

downward 20 mV/step V_{gs} sweeps. Both sweeps reach very close of the room-temperature Boltzmann SS limit of 60 mV/decade. In Fig. 4(a), for downward sweep of V_{gs}, an SS value of ~67.2 mV/decade was achieved near $I_d \sim 10^{-4}$ mA/mm. The SS value was nearly independent of the applied drain bias V_{ds} in the downward V_{gs} sweep. The upward sweep in Fig. 4(b) shows a slightly larger V_{ds} dependence of the SS, yet a similar near-Boltzmann lower value of 66.5 mV/decade is obtained at $V_{ds} = 1$ V. These SS values indicate an interface trap density of $D_{it} = 8 \times 10^{11}$ cm^{-2}eV^{-1}. The low SS values, even at high drain bias voltages, indicate that AlYN can serve as an attractive epitaxial barrier layer for the next generation of GaN HEMTs. However, a more detailed analysis of AlYN/GaN interface quality and trap density using techniques such as transmission electron microscopy (TEM) and frequency, temperature-dependent C–V measurements is needed for this emerging barrier material.

To conclude, in this work, we realized the operation of MOCVD-grown AlYN/GaN HEMTs. Using regrown n$^+$GaN Ohmic contacts to the polarization-induced 2DEG, excellent HEMT DC performance with a low threshold voltage, a saturation drain current exceeding 400 mA/mm, and a transconductance greater than 300 mS/mm are obtained. The AlYN/GaN HEMT exhibited near-ideal sub-threshold swing minimum values of ~66–67 mV/decade, highlighting excellent electrostatic gate control of the 2DEG channel conductivity due to a low interface trap density. Though further studies are necessary to reduce the on-resistance, the high on/off ratio of (>10^9), minimal hysteresis, and DIBL of ~9 mV/V emphasize the stability and reliability of the devices. These results highlight the immense potential of epitaxial AlYN barrier layers in future GaN-based HEMTs for high-performance, high-efficiency, and high-frequency applications in next-generation wireless communication and power electronics systems.

This work was supported in part by the Ultra Materials for a Resilient Energy Grid (regrown contacts and AFM), an Energy Frontier Research Center funded by the U.S. Department of Energy, Office of Science, Basic Energy Sciences under Award #DE-SC0021230, in part by SUPREME, one of seven centers in JUMP 2.0, a Semiconductor Research Corporation (SRC) program sponsored by DARPA (device fabrication) and in part by ARO Grant #W911NF2220177 (device characterization). This work used the Cornell Center for Materials Research (CCMR) Shared Facilities, which are supported by the NSF MRSEC program (DMR-1719875). The authors acknowledge the use of the Cornell NanoScale Facility (CNF), a member of the National Nanotechnology Coordinated Infrastructure (NNCI), which is supported by the National Science Foundation (NSF Grant NNCI-2025233).

AUTHOR DECLARATIONS

Conflict of Interest

The authors have no conflicts to disclose.

Author Contributions

Kazuki Nomoto and Isabel Streicher contributed equally to this work.

Kazuki Nomoto: Conceptualization (equal); Data curation (equal); Formal analysis (equal); Investigation (equal); Methodology (equal); Writing – original draft (equal); Writing – review & editing (equal). **Isabel Streicher:** Conceptualization (equal); Data curation (equal); Investigation (equal); Methodology (equal); Writing – original draft (equal); Writing – review & editing (equal). **Thai-Son Nguyen:** Conceptualization (equal); Data curation (equal); Formal analysis (equal); Investigation (equal); Methodology (equal); Writing – review & editing (equal). **Chandrashekhar Savant:** Conceptualization (equal); Data curation (equal); Formal analysis (equal); Writing – review & editing (equal). **Madhav Ramesh:** Data curation (equal); Formal analysis (equal); Writing – review & editing (equal). **Siyuan Ma:** Formal analysis (equal); Software (equal); Writing – review & editing (equal). **Jimy Encomendero:** Formal analysis (supporting); Methodology (supporting); Software (equal); Validation (equal); Writing – review & editing (equal). **Lutz Kirste:** Conceptualization (equal); Data curation (equal); Investigation (equal); Methodology (equal); Validation (equal); Writing – review & editing (equal). **Patrik Straňák:** Conceptualization (equal); Data curation (equal); Formal analysis (equal); Investigation (equal); Writing – review & editing (equal). **Rüdiger Quay:** Conceptualization (equal); Investigation (equal); Supervision (equal); Writing – review & editing (equal). **Stefano Leone:** Conceptualization (equal); Data curation (equal); Funding acquisition (lead); Project administration (lead); Supervision (equal); Writing – review & editing (equal). **Huili Grace Xing:** Conceptualization (equal); Funding acquisition (equal); Investigation (equal); Project administration (equal); Resources (equal); Supervision (equal); Writing – review & editing (equal). **Debdeep Jena:** Conceptualization (equal); Funding acquisition (equal); Project administration (equal); Resources (equal); Supervision (equal); Writing – review & editing (equal).

DATA AVAILABILITY

The data that support the findings of this study are available from the corresponding author upon reasonable request.

REFERENCES

[1] M. Asif Khan, J. N. Kuznia, A. R. Bhattarai, and D. T. Olson, "Metal semiconductor field effect transistor based on single crystal GaN," Appl. Phys. Lett. **62**, 1786–1787 (1993).

06 June 2025 13:06:53

Published under an exclusive license by AIP Publishing

[2]M. Khan, Q. Chen, M. Shur, B. Dermott, J. Higgins, J. Burm, W. Schaff, and L. Eastman, "Short-channel GaN/AlGaN doped channel heterostructure field effect transistors with 36.1 cutoff frequency," Electron. Lett. **32**, 357–358 (1996).

[3]O. Ambacher, B. Foutz, J. Smart, J. R. Shealy, N. G. Weimann, K. Chu, M. Murphy, A. J. Sierakowski, W. J. Schaff, L. F. Eastman, R. Dimitrov, A. Mitchell, and M. Stutzmann, "Two dimensional electron gases induced by spontaneous and piezoelectric polarization in undoped and doped AlGaN/GaN heterostructures," J. Appl. Phys. **87**, 334–344 (2000).

[4]L. Eastman and U. Mishra, "The toughest transistor yet [GaN transistors]," IEEE Spectr. **39**, 28–33 (2002).

[5]U. Mishra, P. Parikh, and Y.-F. Wu, "AlGaN/GaN HEMTs—An overview of device operation and applications," Proc. IEEE **90**, 1022–1031 (2002).

[6]Y. Cao and D. Jena, "High-mobility window for two-dimensional electron gases at ultrathin AlNGaN heterojunctions," Appl. Phys. Lett. **90**, 182112 (2007).

[7]T. Zimmermann, D. Deen, Y. Cao, J. Simon, P. Fay, D. Jena, and H. G. Xing, "AlN/GaN insulated-gate HEMTs with 2.3 A/mm output current and 480 mS/mm transconductance," IEEE Electron Device Lett. **29**, 661–664 (2008).

[8]K. Shinohara, D. Regan, A. Corrion, D. Brown, Y. Tang, J. Wong, G. Candia, A. Schmitz, H. Fung, S. Kim, and M. Micovic, "Self-aligned-gate GaN-HEMTs with heavily-doped n^+-GaN ohmic contacts to 2DEG," in *International Electron Devices Meeting* (IEEE, 2012), pp. 27.2.1–27.2.4.

[9]M. Gonschorek, J.-F. Carlin, E. Feltin, M. A. Py, and N. Grandjean, "High electron mobility lattice-matched AlInNGaN field-effect transistor heterostructures," Appl. Phys. Lett. **89**, 062106 (2006).

[10]D. Jena, R. Page, J. Casamento, P. Dang, J. Singhal, Z. Zhang, J. Wright, G. Khalsa, Y. Cho, and H. G. Xing, "The new nitrides: Layered, ferroelectric, magnetic, metallic and superconducting nitrides to boost the GaN photonics and electronics eco-system," Jpn. J. Appl. Phys. **58**, SC0801 (2019).

[11]J. Casamento, K. Nomoto, T.-S. Nguyen, H. Lee, C. Savant, L. Li, A. Hickman, T. Maeda, Y.-T. Shao, J. Encomendero, V. Gund, T. Vasen, S. Afroz, D. Hannan, D. A. Muller, H. G. Xing, and D. Jena, "AlScN high electron mobility transistors: Integrating high piezoelectric, high K dielectric, and ferroelectric functionality," in *IEEE BiCMOS and Compound Semiconductor Integrated Circuits and Technology Symposium (BCICTS)* (IEEE, 2023), pp. 132–136.

[12]C. Savant, T.-S. Nguyen, K. Nomoto, S. Vishwakarma, S. Ma, A. Dhar, Y.-H. Chen, J. Casamento, D. J. Smith, H. G. Xing *et al.*, "Epitaxial high-K barrier AlBN/GaN HEMTs," Appl. Phys. Lett. **126**, 1–7 (2025).

[13]T. E. Kazior, E. M. Chumbes, B. Schultz, J. Logan, D. J. Meyer, and M. T. Hardy, "High power density ScAlN-based heterostructure FETs for mm-wave applications," in *IEEE MTT-S International Microwave Symposium (IMS)* (IEEE, 2019), pp. 1136–1139.

[14]S. Krause, I. Streicher, P. Waltereit, L. Kirste, P. Brückner, and S. Leone, "AlScN/GaN HEMTs grown by metal-organic chemical vapor deposition with 8.4 W/mm output power and 48% power-added efficiency at 30 GHz," IEEE Electron Device Lett. **44**, 17–20 (2023).

[15]A. J. Green, J. K. Gillespie, R. C. Fitch, D. E. Walker, M. Lindquist, A. Crespo, D. Brooks, E. Beam, A. Xie, V. Kumar, J. Jimenez, C. Lee, Y. Cao, K. D. Chabak, and G. H. Jessen, "ScAlN/GaN high-electron-mobility transistors with 2.4-A/mm current density and 0.67-S/mm transconductance," IEEE Electron Device Lett. **40**, 1056–1059 (2019).

[16]J. Casamento, T.-S. Nguyen, Y. Cho, C. Savant, T. Vasen, S. Afroz, D. Hannan, H. G. Xing, and D. Jena, "Transport properties of polarization-induced 2D electron gases in epitaxial AlScN/GaN heterojunctions," Appl. Phys. Lett. **121**, 192101 (2022).

[17]J. Casamento, K. Nomoto, T. Nguyen, H. Lee, C. Savant, L. Li, A. Hickman, T. Maeda, J. Encomendero, V. Gund *et al.*, "FerroHEMTs: High-current and high-speed all-epitaxial AlScN/GaN ferroelectric transistors," in *International Electron Devices Meeting (IEDM)* (IEEE, 2022), pp. 11–16.

[18]T.-S. Nguyen, K. Nomoto, W. Zhao, C. Savant, H. G. Xing, and D. Jena, "Strain-balanced AlScN/GaN HEMTs with f_T/f_{MAX} of 173/321 GHz," in *IEEE International Electron Devices Meeting (IEDM)* (IEEE, 2024).

[19]K. Nomoto, J. Casamento, T.-S. Nguyen, L. Li, H. Lee, C. Savant, A. L. Hickman, T. Maeda, J. Encomendero, V. Gund *et al.*, "AlScN/GaN HEMTs with 4 a/mm on-current and maximum oscillation frequency $>$ 130 GHz," Appl. Phys. Express **18**, 016506 (2025).

[20]D. Wang, S. Mondal, P. Kezer, M. Hu, J. Liu, Y. Wu, P. Zhou, T. Ma, P. Wang, D. Wang, J. T. Heron, and Z. Mi, "Band alignment and charge carrier transport properties of YAlN/III-nitride heterostructures," Appl. Surf. Sci. **637**, 157893 (2023).

[21]I. Streicher, P. Straňák, L. Kirste, M. Prescher, S. Müller, and S. Leone, "Two-dimensional electron gases in AlYN/GaN heterostructures grown by metal–organic chemical vapor deposition," APL Mater. **12**, 051109 (2024).

[22]See https://dockchemicals.com for "Dockweiler Chemicals."

[23]S. Leone, I. Streicher, M. Prescher, P. Straňák, and L. Kirste, "Metal-organic chemical vapor deposition aluminum yttrium nitride," Phys. Status Solidi RRL **17**, 2300091 (2023).

[24]I. Streicher, S. Leone, L. Kirste, C. Manz, P. Straňák, M. Prescher, P. Waltereit, M. Mikulla, R. Quay, and O. Ambacher, Phys. Status Solidi RRL **17**, 2200387 (2023).

[25]I. Streicher, S. Leone, M. Zhang, T. S. Tlemcani, M. Bah, P. Straňák, L. Kirste, M. Prescher, A. Yassine, D. Alquier, and O. Ambacher, "Understanding interfaces in AlScN/GaN heterostructures," Adv. Funct. Mater. **34**, 2403027 (2024).

[26]S. Leone, F. Benkhelifa, L. Kirste, C. Manz, S. Mueller, R. Quay, and T. Stadelmann, Phys. Status Solidi (B) **255**, 1700377 (2018).

[27]I. Streicher, S. Leone, C. Manz, L. Kirste, M. Prescher, P. Waltereit, M. Mikulla, R. Quay, and O. Ambacher, "Effect of AlN and AlGaN interlayers on AlScN/GaN heterostructures grown by metal–organic chemical vapor deposition," Cryst. Growth Des. **23**, 782–791 (2023).

[28]L. Li, K. Nomoto, M. Pan, W. Li, A. Hickman, J. Miller, K. Lee, Z. Hu, S. J. Bader, S. M. Lee, J. C. M. Hwang, D. Jena, and H. G. Xing, "GaN HEMTs on Si with regrown contacts and cutoff/maximum oscillation frequencies of 250/204 GHz," IEEE Electron Device Lett. **41**, 689–692 (2020).

[29]J. Guo, Y. Cao, C. Lian, T. Zimmermann, G. Li, J. Verma, X. Gao, S. Guo, P. Saunier, M. Wistey, D. Jena, and H. G. Xing, "Met.-face InAlN/AlN/GaN high electron mobility transistors with regrown ohmic contacts by molecular beam epitaxy," Physica Status Solidi (a) **208**, 1617–1619 (2011).

06 June 2025 13:06:53

Published under an exclusive license by AIP Publishing